Cyclic Peptide Inhibitors of HIV-1 Capsid-Human Lysyl-tRNA Synthetase Interaction

Varun Dewan,[†,§,∥,○] Tao Liu,[†,○] Kuan-Ming Chen,[⊥] Ziqing Qian,[‡] Yong Xiao,[¶] Lawrence Kleiman,[¶] Kiran V. Mahasenan,[#] Chenglong Li,[#] Hiroshi Matsuo,[⊥] Dehua Pei,[†,‡,*] and Karin Musier-Forsyth[†,‡,§,∥,*]

[†]Ohio State Biochemistry Program, [‡]Department of Chemistry and Biochemistry, [§]Center for RNA Biology, [∥]Center for Retroviral Research, and [#]Division of Medicinal Chemistry & Pharmacognosy, The Ohio State University, Columbus, Ohio 43210, United States

[⊥]Biochemistry, Molecular Biology and Biophysics, University of Minnesota, Minneapolis, Minnesota 55455, United States

[¶]Lady Davis Institute for Medical Research and McGill AIDS Centre, Jewish General Hospital, Montreal, Quebec, Canada H3T 1E2

Ⓢ *Supporting Information*

ABSTRACT: The human immunodeficiency virus type 1 (HIV-1) capsid protein (CA) plays a critical role in the viral life cycle. The C-terminal domain (CTD) of CA binds to human lysyl-tRNA synthetase (hLysRS), and this interaction facilitates packaging of host cell tRNA^{Lys,3}, which serves as the primer for reverse transcription. Here, we report the library synthesis, high-throughput screening, and identification of cyclic peptides (CPs) that bind HIV-1 CA. Scrambling or single-residue changes of the selected peptide sequences eliminated binding, suggesting a sequence-specific mode of interaction. Two peptides (CP2 and CP4) subjected to detailed analysis also inhibited hLysRS/CA interaction *in vitro*. Nuclear magnetic resonance spectroscopy and mutagenesis studies revealed that both CPs bind to a site proximal to helix 4 of the CA-CTD, which is the known site of hLysRS interaction. These results extend the current repertoire of CA-binding molecules to a new class of peptides targeting a novel site with potential for development into novel antiviral agents.
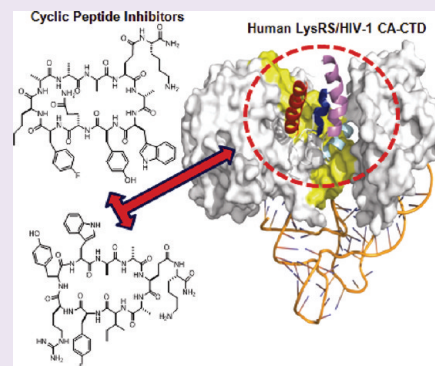
<p style="text-align: justify">
Human immunodeficiency virus type 1 (HIV-1) infection involves several key steps throughout the viral life cycle, which are mediated by protein−protein and protein−nucleic acid interactions. Highly active antiretroviral therapy against HIV-1 consists of administering a cocktail of inhibitors that target key players in viral pathogenesis, including the virally encoded enzymes reverse transcriptase, integrase, and protease, along with inhibitors of viral entry.[1−3] Although successful results have been achieved by combination therapy, complete eradication of HIV-1 has been a challenge, primarily due to the emergence of drug resistant strains.[4] Identification of alternative targets for restriction by novel and potent antiviral compounds is therefore needed. The critical role played by HIV-1 capsid protein (CA) throughout the viral life cycle makes it an attractive target for antiviral intervention.[5−7]
</p>

HIV-1 CA is one of the major domains of the large viral precursor proteins Gag and GagPol, which interact with each other, with the viral RNA genome, and with various host cell factors during viral assembly.[8] The CA domain mediates Gag-Gag interactions that are critical for immature particle formation.[9] CA is a two-domain dimeric protein, composed of largely helical N-terminal and C-terminal domains (NTD and CTD, respectively) separated by a flexible linker.[10] The CTD contains the dimerization motif and plays an important role in Gag multimerization.[11,12] Using crystallographic studies, the dimer interface of CA has been mapped to helix 2 of the

CTD with residues Trp184 and Met185 providing the major stabilizing contacts.[13]

Upon proteolytic processing, the CA protein is released from the Gag precursor and rearranges to form a conical core surrounding the viral RNA genome and associated proteins.[10,14] Uncoating of the viral core, which occurs following entry into target cell and concomitant with early steps of reverse transcription,[15] is another key step in the viral life cycle. Mutations that alter the core stability lead to dramatic reductions in viral infectivity.[12,16] The stability of the CA core is dependent on inter- as well as intramolecular interactions between the NTD and the CTD of CA.[17] The NTD (residues 1−146) forms hexamers and the CTD (residues 146−231), which is dimeric in solution, links adjacent hexamers.[11] Thus, potential therapeutic strategies include disrupting CA−CA interactions involved in immature particle formation, mature core assembly, or core disassembly.

HIV-1 CA is also known to interact with a variety of host cell factors[6] including cyclophilin A, a host restriction factor TRIM5α, and human lysyl-tRNAsynthetase (hLysRS). In the immature virus particle, host cell tRNA^{Lys,3} is annealed to the

genomic RNA *via* complementary base-pairing interactions and serves as a primer for reverse transcription.[18,19] Gag specifically interacts with hLysRS *via* its CA domain and packages it into the newly budding virions.[20] This interaction is important for selective packaging of primer tRNA[Lys] into the virion.[8] A recent report suggests that interactions also occur between LysRS and the Pol domain of the GagPol precursor.[21] The packaging of hLysRS into HIV-1 is specific; out of nine aminoacyl-tRNA synthetases and three additional components of the mammalian multisynthetase complex tested, only LysRS has been shown to be packaged.[22] Previously, we have mapped the interaction interface to helix 4 (h4) of the CA-CTD and motif 1 of hLysRS, which are also the homodimerization domains of the individual proteins.[23] Furthermore, monomeric LysRS and monomeric Gag have also been shown to interact *in vitro* with a similar affinity as the wild-type (WT) proteins.[24] More recently, Schimmel and co-workers have produced an *ab initio* energy minimized "bridging monomer" model of the HIV-1 CA-CTD/hLysRS/tRNA[Lys] ternary complex[25] (Figure 1). Furthermore,
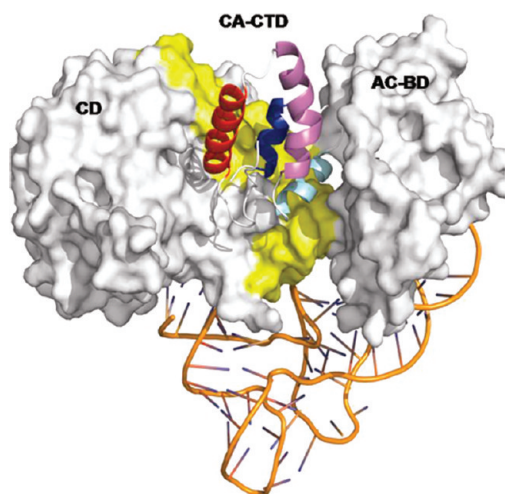

Figure 1. Model of the tRNA[Lys] (orange), hLysRS (gray), and HIV-1 CA-CTD (multicolor) complex. This figure is based on the "bridging monomer" model published by Guo *et al.*[25] The motif 1 dimerization domain of hLysRS is yellow, and the helices of CA-CTD are red (h1), pink (h2), cyan (h3), and blue (h4). Also indicated is the anticodon binding domain (AC-BD) and the catalytic domain (CD) of LysRS. The N-terminal 65 amino acids of hLysRS are not shown.

circular dichroism experiments along with *in silico* binding studies support an interaction between h4 of the CA-CTD and helix 7 of the motif 1 domain of hLysRS.[26] Taken together, these data suggest that targeting the h4 region of the CA-CTD, which forms the interface with hLysRS, is another potential drug target.

Previous attempts to develop inhibitors against CA led to the identification of a variety of small molecule inhibitors, namely, CAP-1,[27] CAP-2,[27] PA-457,[28] and PF-3450074.[29] A 12-mer peptide known as the CA assembly inhibitor (CAI) was identified by phage-display screening and reported to disrupt the assembly of both immature and mature virus-like particles *in vitro* by binding to the CA-CTD.[30] However, it lacked cell permeability and failed to inhibit HIV-1 in cell culture. An improved variant of the CAI peptide was generated by "hydrocarbon stapling", and the resulting peptide, NYAD-1,[31] disrupted formation of both immature and mature virus-like particles in cell-free and cell-based *in vitro* assembly assays.

Furthermore, rationally designed interfacial peptide inhibitors of CA have also been shown to possess antiviral activity.[32] This study further validates CA as an anti-HIV drug target.

In this work, we employed a combinatorial library approach to identify cyclic peptides (CPs) that bind to HIV-1 CA. CPs are a distinct class of biologically active compounds[33] that are widely produced in nature by plants, bacteria, fungi, marine invertebrates, and primate leukocytes. CPs such as cyclosporin A[34] (an immunosuppressant), caspofungin[35] (an antifungal agent), and daptomycin[36] (an antibiotic) are clinically used as therapeutic agents. In comparison to their linear counterparts, CPs are more stable against proteolytic degradation due to their higher conformationally rigidity and lack of free N- or C-termini. The entropic advantages associated with increased rigidity also make CPs potentially tighter-binding and more specific ligands of macromolecular targets.[33] Recently, conformationally constrained CP mimics of the HIV-1 trans-activator of transcription (Tat) have been used to block Tat interactions with the trans-activation response element RNA at nanomolar concentrations *in vitro*.[37]

We report here the synthesis, high-throughput screening, and identification of novel CP ligands against HIV-1 CA. The most promising peptides (CP2 and CP4) bound with ~500 nM affinity and inhibited the LysRS/CA interaction with IC_{50} values of ~1 μM *in vitro*. Furthermore, NMR studies along with mutational analysis suggest that both peptides bind to the site on the CA-CTD that has been previously identified as the site of LysRS interaction.[23,25] Taken together, these results suggest that CPs represent a new class of CA-CTD binders that could be further exploited for antiviral drug development.

RESULTS AND DISCUSSION

Previous studies have characterized the interaction between HIV-1 CA-CTD and hLysRS, which is critical for tRNA primer packaging into HIV-1. This complex represents a novel target for antiviral intervention, and we hypothesize that CPs can be identified to block this viral protein−host protein interaction. In this work, we use a chemical approach, namely, combinatorial library synthesis followed by high-throughput screening, to identify CPs that bind to HIV-1 CA. Detailed biochemical analyses are then performed to characterize their binding affinity, sequence specificity, target selectivity, and ability to inhibit LysRS interaction. Biophysical and genetic studies to identify the binding pocket are also carried out.

Design and Synthesis of CP Library. A one-bead-two-compound (OBTC) CP library was synthesized (Supporting Figure s1a) containing five random residues, cyclo-[aX^{1}X^{2}X^{3}X^{4}X^{5}a$_{(0-3)}$E]BBNBRM-resin (where "a" is D-alanine, B is β-alanine, and X represents the random residues) (Supporting Methods, Supporting Figure s1b). Each bead was spatially segregated into two layers, with a unique CP displayed on the surface layer and the corresponding linear peptide contained in the bead interior as a coding tag. The library was constructed to have a 10-fold reduced ligand density on the bead surface relative to the loading of linear peptides inside the bead. We and others have previously shown that a lower density on the bead surface increases the screening stringency, allowing the identification of the most active ligands by greatly reducing the amount of nonspecific binding caused by avidity effects.[38,39] The density of linear peptide inside the bead was kept high to provide enough material for sequencing. Each of the random positions contained 26 amino acids including 12 proteinogenic α-L-amino acids [Arg, Asp, Gln, Gly, His, Ile, Lys,

Pro, Ser, Thr, Trp, and Tyr], four non-proteinogenic α-L-amino acids [Fpa, Nle, Orn, Phg], six α-D-amino acids [D-Ala, D-Asn, D-Glu, D-Leu, D-Phe, and D-Val], and four N^{α}-methylated α-L-amino acids [Mal, Mle, Mpa, Sar] (see Supporting Table s1). D-Alanine was added to the N-terminus of all peptides to give more uniform cyclization efficiency, while different numbers of D-alanine were added to the C-terminal side of the random sequence to give different ring sizes (hepta-, octa-, nona-, and decapeptides).

Library Screening against CA and WM CA-CTD. A portion of the CP library (100 mg, ~3 × 10^5 beads) was screened against Texas Red-labeled CA and a non-dimerizing CA-CTD variant (W184A-M185A CA-CTD)[40] in two stages. Initial screening against CA resulted in 39 fluorescent beads. Fifty non-fluorescent beads were randomly selected from the first screen as controls. Both "hits" and control beads were washed with 8 M guanidine·HCl to remove the bound proteins and subjected to a second round of screening against WM CA-CTD. Of the 39 initial hits, 21 beads again developed a strong fluorescence signal (Supporting Figure s2), while only 4 beads in the control group displayed weak fluorescence. The 21 hits were sequenced by partial Edman degradation/mass spectrometry (PED/MS) (Supporting Table s1). Inspection of the selected peptides revealed a preference for hydrophobic residues in the randomized positions and larger ring sizes, although CPs of varying ring sizes (7−10 amino acids) were selected.

CP2 and CP4 Bind CA with High Affinity. To quantify the binding affinity between the CPs and CA, the six most potent hits based on fluorescence intensity (CP1−CP6) were individually resynthesized with the addition of a lysine residue to the side chain of the invariant glutamate (Table 1). This

Table 1. Sequences of Selected CPs and Apparent Dissociation Constants (K_d) for Binding to CA and WM CA-CTD Based on FA Measurements[a]

peptide	sequence	K_d (μM) CA	K_d (μM) WM CA-CTD
CP1	cyclo(D-Ala-D-**Phe**-D-**Phe**-Ile-Arg-**Trp**-D-Ala-D-Ala-D-Ala-Glu)-Lys	ND	ND
CP2	cyclo(D-Ala-**Trp-Tyr-Gln-Fpa-Nle**-D-Ala-D-Ala-D-Ala-Glu)-Lys	1.1 ± 0.1	0.40 ± 0.05
CP3	cyclo(D-Ala-**Thr-Tyr-Tyr-Trp-Phg**-D-Ala-D-Ala-D-Ala-Glu)-Lys	4.4 ± 1.2	ND
CP4	cyclo(D-Ala-**Ile-Fpa-Arg-Tyr-Trp**-D-Ala-D-Ala-Glu)-Lys	0.35 ± 0.01	0.46 ± 0.04
CP5	cyclo(D-Ala-**Arg-Tyr-Arg-Trp-Fpa**-D-Ala-Glu)-Lys	1.8 ± 0.3	1.6 ± 0.2
CP6	cyclo(D-Ala-D-**Phe-Arg-Fpa-Mpa-Trp**-Glu)-Lys	5.3 ± 1.9	1.7 ± 0.2
SCP2	cyclo(D-Ala-**Gln-Nle-Tyr-Trp-Fpa**-D-Ala-D-Ala-D-Ala-Glu)-Lys	NB	NB
SCP4	cyclo(D-Ala-**Tyr-Ile-Trp-Arg-Fpa**-D-Ala-D-Ala-Glu)-Lys	NB	NB

[a]Measurements were performed in the presence of binding buffer as described in the Methods. Reported values are averages of three trials with the standard deviation indicated. ND, could not be determined accurately due to a low FA. NB, no binding observed. Highlighted in bold are the variable positions of each CP.

lysine side chain provides a handle for labeling with fluorescein or biotin. The binding affinity of CP1−CP6 to CA and WM

CA-CTD was determined by fluorescence anisotropy (FA). With the exception of CP1 and CP3, most of the selected peptides bound to both target proteins. Among them, CP2 and CP4 had the highest affinity, with K_d values of 0.4−1.1 μM (Table 1 and Figure 2a). The affinity of CP1 for the proteins or
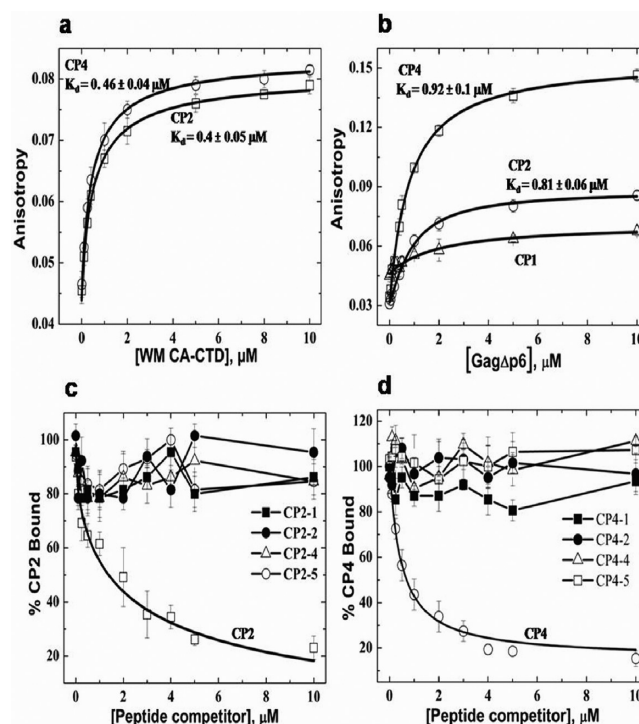

Figure 2. FA assay of CP binding to WM CA-CTD and GagΔp6. (a) Plots of FA as a function of WM CA-CTD concentration for fluorescein-labeled CP2 and CP4 (100 nM each). (b) The binding of GagΔp6 to fluorescein-labeled CP1, CP2, and CP4 (100 nM each). (c) Competition between fluorescein-labeled CP2 (100 nM) and unlabeled CP2 and its Asn-scan variants (0−10 μM) for binding to WM CA-CTD (2 μM) (Supporting Table s4). (d) Competition between fluorescein-labeled CP4 (100 nM) and unlabeled CP4 and its Asn-scan variants (0−10 μM) for binding to WM CA-CTD (2 μM).

that of CP3 for WM CA-CTD could not be accurately determined due to low FA signals, suggesting that the interactions are rather weak. We also tested the binding of CP1, CP2, and CP4 to HIV-1 GagΔp6, a truncated form of Gag lacking the C-terminal p6 domain. CP2 and CP4 bound with apparent K_d values of ~0.8−0.9 μM (Figure 2b), whereas CP1 failed to show significant binding. CP2 and CP4 also bound to WT CA-CTD with K_d values of 0.37−0.52 μM (Supporting Figure s4a). Furthermore, surface plasmon resonance (SPR) experiments confirmed the binding of CA and WM CA-CTD to biotinylated CP2 and CP4 peptides immobilized onto a streptavidin-coated surface and gave K_d values (0.06−1.3 μM) similar to those derived from the FA assay (Supporting methods, Supporting Table s3).

To determine the binding stoichiometry, we performed an FA assay by using saturating concentrations of WM CA-CTD and CP2 or CP4 (structures shown in Figure 3a and b). Increasing amounts of WM CA-CTD (0−1.2 mM) were titrated against a fixed concentration of CP2/CP4 (0.6 mM), and binding was assayed by monitoring changes in anisotropy of trace amounts of fluorescein-labeled CP2/CP4. In both cases, the amount of bound CP2/CP4 peptide increased
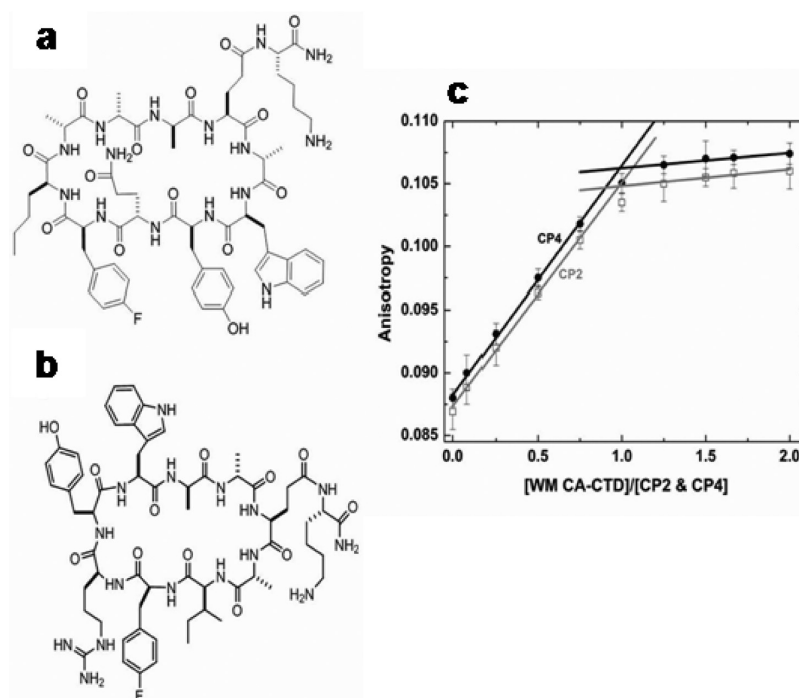
Figure 3. Structures of (a) CP2 and (b) CP4. (c) FA assay to determine the binding stoichiometry of CP2 and CP4 to WM CA-CTD. Increasing WM CA-CTD was added to a mixture of 10 μM fluorescein-labeled CP2 or CP4 and 590 μM unlabeled CP2 or CP4 in binding buffer (see Methods). Binding stoichiometry was obtained by determining the intersection of the linear fits to the first 5 data points and the last 4 data points.

linearly with the protein concentration until the protein/peptide ratio reached 1:1, when the amount of WM CA-CTD·CP complex plateaued, supporting a 1:1 binding stoichiometry (Figure 3c).

To determine whether the CPs are specific for HIV-1 CA, we tested their binding to HIV-1 nucleocapsid (NC), matrix (MA), hLysRS, human prolyl-tRNAsynthetase (hProRS), and *Escherichia coli* cysteinyl-tRNA synthetase (EcCysRS) by FA. As shown in Supporting Table s2, the CPs bound many of the proteins with micromolar (μM) affinities. The hydrophobic nature of the CPs is likely responsible for the observed non-selective binding. To check for their sequence specificity in binding to CA or WM CA-CTD, two control peptides (SCP2 and SCP4) were synthesized containing scrambled sequences of CP2 and CP4 (Table 1). Both scrambled peptides failed to bind CA or WM CA-CTD. We next performed an "asparagine scan", wherein the hydrophobic residues at variable positions 1, 2, 4, and 5 were individually replaced with Asn, to identify the residues critical for CA binding and obtain a less hydrophobic variant (which may be more selective for CA) (Supporting Table s4). Strikingly, substitution of Asn for any of the hydrophobic residues greatly reduced the binding affinity. In a FA competition assay, CP2 and CP4 inhibited the binding of fluorescein-labeled CP2 or CP4 to WM CA-CTD with IC$_{50}$ values of 1.2 and 0.63 μM, respectively (Figure 2c and d). In contrast, none of the Asn-scan variants (at 10 μM) showed significant competition. Taken together, these data suggest that CP2 and CP4 (Figure 3a and b) are high-affinity ligands of WM CA-CTD/CA and bind in a sequence-dependent manner. Based on the sequence of the selected CPs and the results of the Asn scan, both CP2 and CP4 appear to bind CA primarily *via* hydrophobic interactions, which is consistent with the hydrophobic nature of the protein surface.[11,17,41]

Inhibition of CA-LysRS Interaction by CP2 and CP4. We have previously shown that hLysRS specifically interacts with HIV-1 CA,[24] GagΔp6,[24] and CA-CTD[23] *in vitro*. We assessed the ability of the CPs to inhibit this interaction by carrying out an FA competition assay (Supporting methods), in which the binding of Texas Red-labeled CA or WM CA-CTD to hLysRS was examined in the absence and presence of increasing amounts of CP (Figure 4a). CP2 and CP4 readily inhibited the binding of hLysRS to both CA (Figure 4b) and WM CA-CTD (Figure 4c) with IC$_{50}$ values of 0.5−1.0 μM, whereas no inhibition or much weaker inhibition was observed for CP1, CP3, CP5, and CP6 (Table 2). Thus, the latter peptides, which have lower affinity for CA (Table 1), may also bind to CA at a site distinct from the hLysRS binding site.[23,25] CP2 and CP4 also inhibited the interaction of hLysRS with GagΔp6, with IC$_{50}$ of ~1−1.5 μM, whereas CP1 showed only slight inhibition (Figure 4d).

Identification of CP Binding Surface by NMR and Mutational Analysis. To map the CP binding site on WM CA-CTD, three peptides were chosen for NMR analysis: CP2, CP4, and a control hydrophilic CP (CPX).[42] The peptides were labeled at the terminal lysine moiety using the amine-reactive spin-label 1-oxyl-2,2,5,5-tetramethylpyrroline-3-carboxylate *N*-hydroxysuccinimide ester prior to purification. We first tested the binding of CPX to either CA or WM CA-CTD by FA. As shown in Supporting Figure s4b, CPX failed to produce a significant anisotropy change, thereby suggesting very weak or no binding to the target proteins. This result further confirmed the sequence specificity of CP2 and CP4 in binding to CA-CTD *in vitro*.

Paramagnetic relaxation enhancement (PRE) nuclear magnetic resonance (NMR) spectroscopy was performed by using spin-labeled CP2, CP4, CPX, and uniformly ^{15}N-labeled WM CA-CTD (Supporting methods). Titration of spin-labeled CPX
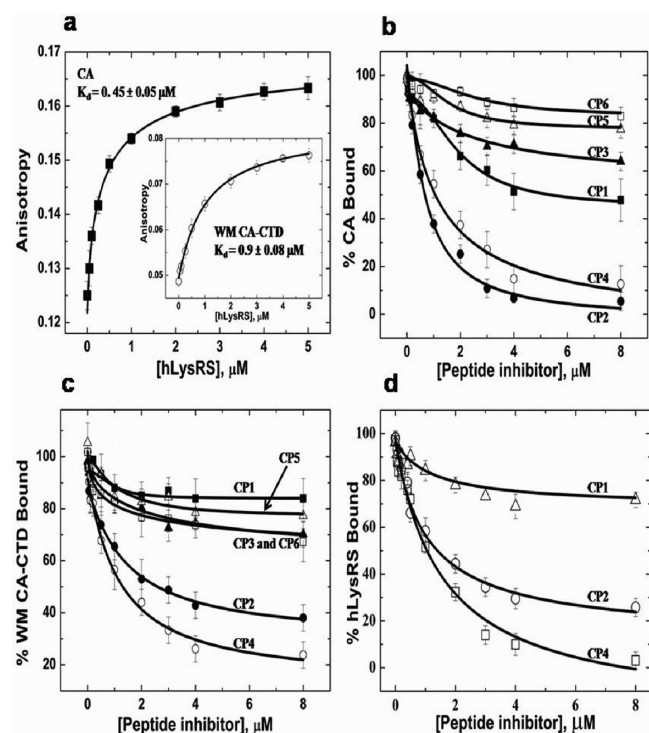
Figure 4. Inhibition of CA-hLysRS interaction by CPs. (a) Binding of Texas Red-labeled hLysRS to CA (100 nM) and WM CA-CTD (inset). (b) Texas Red-labeled CA (100 nM) was preincubated with varying concentrations of CPs (0−8 μM), followed by addition of unlabeled hLysRS (3 μM). (c) Texas Red-labeled WM CA-CTD (100 nM) was preincubated with varying concentrations of CPs (0−8 μM), followed by addition of unlabeled hLysRS (3 μM). (d) GagΔp6 (3 μM) was preincubated with varying amounts of CP1, CP2, and CP4 (0−8 μM) followed by addition of 100 nM FITC-labeled hLysRS.

Table 2. Inhibition of LysRS/CA, LysRS/WM CA-CTD, and LysRS/GagΔp6 Interaction by CP1-CP6

	IC$_{50}$ (μM)^a		
peptide	LysRS/CA	LysRS/WM CA-CTD	LysRS/GagΔp6
CP1	5.3 ± 0.8	NI	NI
CP2	0.61 ± 0.04	0.97 ± 0.1	1.5 ± 0.5
CP3	23 ± 3	16 ± 3	
CP4	0.91 ± 0.1	0.53 ± 0.1	1.1 ± 0.3
CP5	NI	63 ± 40	
CP6	NI	15 ± 3	

^{a}IC$_{50}$ values were determined from FA inhibition measurements as described in Methods. Reported values are averages of three trials with the standard deviation indicated. A dash indicates the experiment was not performed. NI, no significant inhibition observed.

in the presence of 250 μM ^{15}N-labeled WM CA-CTD at a 1:5 protein:peptide ratio failed to produce any significant change in signal intensity, confirming the FA results showing little

interaction with this hydrophilic peptide (Supporting Table s6). In contrast, titration of spin-labeled CP4 at a 1:5 protein:peptide ratio resulted in a significant decrease in signal intensity (>40% reduction) for 14 residues (Table 3). Unfortunately, addition of spin-labeled CP2 to 250 μM WM CA-CTD at a 1:2 protein:peptide ratio caused protein precipitation. An experiment at lower protein concentration (100 μM) was conducted with both CP2 and CP4. Titration of CPs at a 1:5 protein:peptide ratio resulted in a significant decrease in signal intensity for 3 residues: I150, L211, and E212 (Supporting Table s5). On the basis of the data shown in Supporting Table s5 and Table 3, we speculate that CP2 and CP4 bind to similar sites on CA-CTD. As an additional control, we also checked whether the spin-probe alone caused any intensity changes upon incubation with 250 μM ^{15}N-labeled WM CA-CTD at a 1:5 protein:spin-probe ratio. The amine reactive spin-probe was prepared by using excess glycine as a quenching agent. As shown in Supporting Table s7, the decrease in signal intensity caused by the spin-probe alone was small, suggesting that the intensity decreases observed are due to CP binding.

As summarized in Table 3, residues I150, D152, K158, R173, T186, Q192, and G208 showed signal intensity decreases between 40% and 70%, whereas residues T148, L151, V181, A185, L211, E212, and T216 showed signal intensity decreases of >70% (Figure 5a). These results suggest two potential CP binding sites on the protein surface. The first site (Figure 5b and c) lies between the 3$_{10}$ helix and h2 and constitutes eight residues: T148, I150, L151, D152, V181, A185, T186, and Q192. The second site is primarily located on h4 (Figure 5d and e) and comprises residues A208, L211, E212, and T216.

To map the residues involved in binding, we constructed seven point mutants of residues at both sites 1 and 2. Five residues showing the largest decrease in intensity (L151, V181, L211, E212, and T216) and two additional residues (D152 and Q192) were mutated to alanine. These mutant proteins were then tested for binding to fluorescein-labeled CP2 and CP4 by FA. As shown in Figure 5f, the three mutations at the binding site 2 (i.e., L211A, E212A, and T216A) resulted in ~9-, 4-, and 7-fold reduction in binding affinity to CP2, respectively. In comparison, the L151A and V181A variants with mutations in binding site 1 decreased their affinity for CP2 by only ~2-fold. Similar results were obtained with CP4. While three binding site 2 variants exhibited 4- to 12-fold weaker binding, the site 1 variants did not significantly impact CP4 binding. In conclusion, our mutational analysis supports site 2 as the binding site for both CP2 and CP4. Since CP2 and CP4 bind to WM CA-CTD in a 1:1 stoichiometry even at saturating concentrations, we conclude that site 2 was the primary binding site for the CPs.

To further understand the binding mode of CPs, a docked model of CP4 to WM CA-CTD was generated (Supporting Methods and Figure 5g). This model shows key consistency

Table 3. Summary of NMR Data Obtained upon Titration of 250 μM WM CA-CTD with Spin-Labeled CP4^a

	T148	I150	L151	D152	K158	R173	V181	A185	T186	Q192	G208	L211	E212	T216
1:1	53%	54%	43%	87%	68%	93%	54%	66%	82%	63%	87%	40%	69%	60%
1:2	51%	48%	30%	75%	70%	76%	34%	44%	74%	59%	75%	21%	50%	41%
1:5	21%	32%	11%	50%	41%	45%	14%	16%	52%	45%	42%	5%	21%	10%

^{a}Fourteen WM CA-CTD residues showing significant (> 40%) decreases in peak intensity upon titration with spin-labeled CP4 (1:1, 1:2, and 1:5 protein:peptide ratio) are shown. Numbers indicate peak intensity relative to that of the free protein.
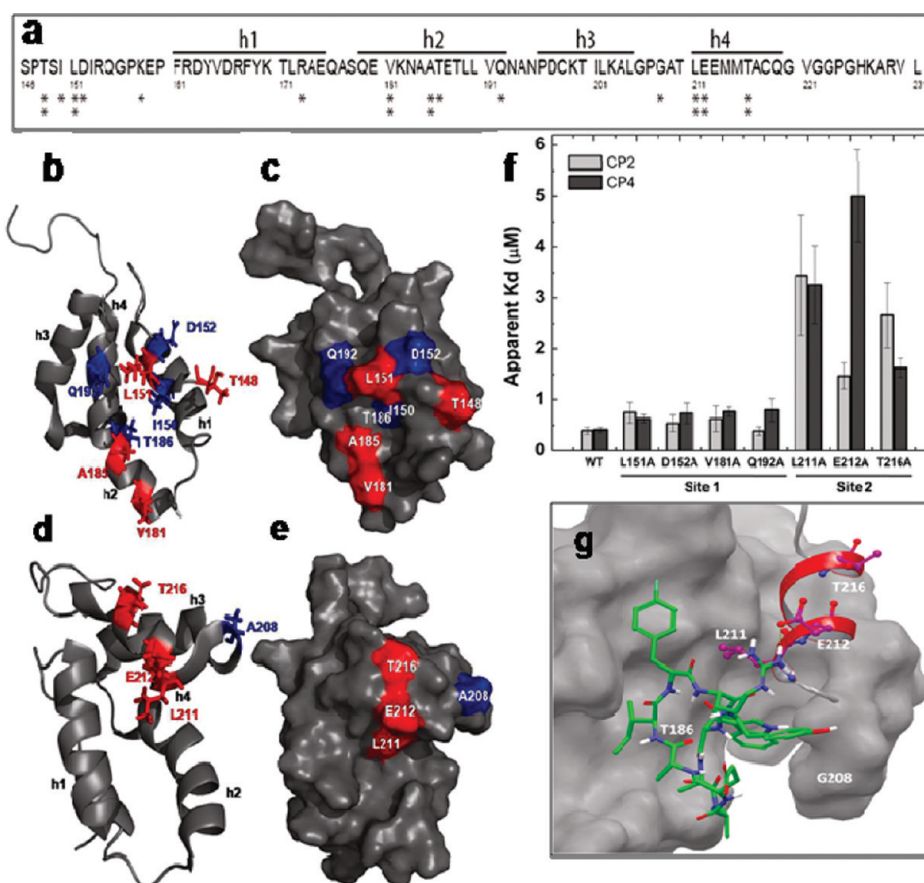
Figure 5. (a) Sequence of WM CA-CTD with 4 helices indicated: h1 (residues 161−175), h2 (residues 179−192), h3 (residues 196−205), and h4 (residues 211−220). Asterisks indicate the residues that display decreased signal intensity upon titration with spin-labeled CP4. One asterisk indicates a 40−70% reduction in signal intensity, while two asterisks indicate a >70% reduction in signal intensity. (b−e) Views of HIV-1 WM CA-CTD (PDB ID: 2K1C) generated by PyMoL[56] showing the two potential binding surfaces of CP4 based on NMR studies using spin-labeled peptide. (b) The eight residues constituting binding site 1 are explicitly shown: T148, I150, L151, D152, V181, A185, T186, and Q192. (c) Surface representation of binding site 1 shown in the same orientation used in panel b. (d) The four residues constituting binding site 2 are explicitly shown: A208, L211, E212, and T216. (e) Surface representation of binding site 2 showed in the same orientation used in panel d. Residues in blue and red displayed 40−70% and >70% reduced signal intensity upon CP4 binding, respectively. (f) Bar graph representation of FA binding analysis using WM CA-CTD point mutants. Fluorescein-labeled CP2 and CP4 (100 nM) were bound to WT WM CA-CTD and variants of binding site 1 (L151A, D152A, V181A, and Q192A) and binding site 2 (L211A, E212A, and T216A). The apparent K_d values are the average of three trials with the standard deviation indicated. (g) Model of CP4 docked onto HIV-1 CA-CTD- X-ray crystal structure (PDB ID: 2BUO). Capsid protein residues are shown as a molecular surface representation except for the h4 residues.

with the experimental data. Arg and Tyr residues of CP4 wrap on the N-terminus of h4 with Arg-E212 ion pair and h4 helical dipole interaction with Tyr side-chain π electrons, affecting the chemical shifts of quite a few h4 residues. Trp, Ile, and Fpa side chains have strong interactions to the CA-CTD binding cleft, affecting chemical shifts of G208, T186, and L211. The interactions are mostly hydrophobic and van der Waals with the CA-CTD binding pocket, which consists of residues Phe168, Leu172, Thr186, Leu190, Val191, and Met214. The subpocket in which Trp occupies is partially covered by the loop residues 206−210. The CP4 Ile and Fpa also mimic the Leu and Tyr residues of CAI[30] peptide helix in their interactions with CA-CTD, respectively.

Conclusion. In this study, screening of an OBTC library identified two CPs that bind to HIV-1 CA-CTD with low micromolar affinity. These novel peptides are also capable of inhibiting the interaction between CA and hLysRS at low micromolar concentrations. PRE NMR spectroscopy studies identified two potential binding pockets. One site involves the N-terminal 3_{10} helix and h2, whereas the second site lies

primarily on h4. Site-directed mutagenesis and computational docking studies are consistent with the second site being directly involved in binding; mutations in this region significantly reduced the CP binding affinity (up to 12-fold reduction in K_d), while changes in site 1 had only minimal (≤2-fold) effects. Overall, the mutagenesis results are in excellent agreement with the previously identified binding site for hLysRS[23,25] and help to explain the *in vitro* inhibition of LysRS-CA binding observed in the presence of these CPs.

The ability of selected peptides CP2, CP4, and a control octa-arginine peptide (R8) to inhibit HIV-1 in cell-based assays was also tested (Supporting Methods). This was accomplished by attaching an octa-arginine tail known to facilitate membrane translocation and a fluorescein probe for monitoring the internalization. Although both CPs were internalized by the cells (Supporting Figure s5), they did not show significant inhibition of HIV-1 replication (Supporting Methods and Supporting Figure s6). Given the ability of the CPs to bind to other proteins *in vitro*, this result was not unexpected. Further modification of the CPs and/or future studies incorporating

negative selection steps into the screening protocol should increase the target protein selectivity.

In summary, we have identified a new class of compounds with the potential to inhibit HIV replication. We demonstrated the feasibility of selecting CPs that bind to CA-CTD with high affinity and in a sequence-dependent manner. CP2 and CP4 bind proximal to the h4 domain of CA-CTD and are, therefore, also effective at inhibiting CA's interaction with one of its known binding partners, hLysRS. Although the selected peptides are not specific for CA (they also bind to other proteins), they demonstrate the feasibility of developing small-molecule inhibitors (such as cyclic peptides) against HIV-1 CA-hLysRS interaction as a novel strategy for anti-HIV therapy. It should be possible to improve the binding affinity and specificity as well as the pharmacokinetic properties of the selected CPs through medicinal chemistry efforts (e.g., replacement of the invariant D-alanine residues with other amino acids).

■ METHODS

Synthesis of Individual CPs. Each peptide (CP1-CP6, SCP2, SCP4, and single Asn variants of CP2 and CP4) was synthesized on 200 mg of Rink Resin LS (0.2 mmol g^{-1}) in a manner similar to that employed for the library synthesis (Supporting methods) except the synthesis was started with a lysine residue followed by the coupling of Fmoc-Glu-OAll for the ring cyclization. Peptide cyclization was monitored by a ninhydrin test to detect any remaining amines. The peptides were released from the resin by reagent K, evaporated to a minimum volume under a nitrogen atmosphere, and triturated three times with cold diethyl ether. The resulting crude peptides were purified by reversed-phase high-performance liquid chromatography (HPLC) on a C$_{18}$ column (Supporting Figure s3), and the authenticity of the peptides was confirmed by matrix-assisted laser desorption/ionization-time of flight mass spectrometry (MALDI-TOF MS) analysis. Fluorescein-labeled and biotinylated peptides were prepared by treating peptides with 3 equiv of 5-carboxyfluorescein or biotin succinimidyl ester in 100 mM sodium bicarbonate buffer (pH 8.5) and dimethyl sulfoxide (DMSO) 1:1 (v/v) mixture with a total reaction volume of 100 μL. The reaction was allowed to proceed at RT for 20 min, and any unreacted dye or biotin ester was quenched by treatment with 5 μL of 1 M Tris-HCl buffer (pH 8.5) for 5 min. The spin-labeled peptides, CP2, CP4, and a control hydrophilic CP with the sequence cyclo-ARYQSRVE (CPX), were prepared similarly using the amine reactive spin label 1-oxyl-2,2,5,5-tetramethylpyrroline-3-carboxylate N-hydroxysuccinimide ester. FITC-labeled octa-arginine containing peptides were prepared as described previously.[43] All labeled peptides were purified and characterized by MS as described above.

Protein Purification and Labeling. The following proteins were overexpressed in E. coli and purified according to previously published procedures: hLysRS,[24] CA,[24,44] WM CA-CTD,[23,24] and GagΔP6.[45] Protein concentrations were estimated using the Bradford assay. Full-length HIV-1 CA and WM CA-CTD were labeled with Texas Red-X, succinimidyl ester following the suggested protocol by Molecular Probes. Briefly, 100 μM protein was incubated with Texas Red-X dye freshly dissolved in anhydrous DMSO, at a 5:1 dye:protein ratio for 60 min at RT in 150 mM NaCl, 40 mM HEPES, pH 7.5. The reaction was quenched by addition of 5 μL of 1 M Tris-HCl, pH 8.5, and unreacted dye was removed by passing the reaction mixture through a column assembly containing the purification resin provided by the manufacturer. The covalent labeling was confirmed by visualizing the fluorescence on a denaturing polyacrylamide gel. The final labeling stoichiometries were determined by measuring the absorbance at 280 and 595 nm and using the following excitation coefficients: ϵ_{280} = 32,095 M^{-1} cm^{-1} (CA), ϵ_{280} = 3,105 M^{-1} cm^{-1} (WM CA-CTD), ϵ_{595} = 80,000 M^{-1} cm^{-1} (Texas Red-X). Labeling stoichiometries for CA and WM CA-CTD were estimated to be 0.8:1 and 1:1 protein:-fluorophore, respectively. 5-Fluorescein isothiocyanate (FITC) label-

ing of CA and hLysRS was performed according to a previously published procedure.[24] Labeling stoichiometries were 0.7:1 and 0.9:1 for CA and hLysRS, respectively.

Library Screening. The library resin (100 mg) was swollen in DCM, washed extensively with DMF, doubly distilled water, and screening buffer (30 mM HEPES, pH 7.4, 150 mM NaCl, 0.05% Tween 20, and 0.1% gelatin), and blocked overnight at 4 °C with 3% bovine serum albumin (BSA) in screening buffer. Texas Red-labeled CA protein was added to the library to a final concentration of 300 nM, and the mixture was incubated in a Petri dish for 6 h at 4 °C with gentle shaking. The library was viewed under an Olympus SZX12 fluorescence microscope (Olympus America) (Supporting Figure s2), and red-colored beads were manually removed from the library with a micropipet. Prior to the next round of screening, the positive beads were extensively washed with screening buffer, double ionized water, 8 M guanidine·HCl, and N,N-dimethylformamide (DMF). Secondary screening experiments were performed in the same way with 500 nM Texas Red-labeled CA-CTD. The positive beads were individually sequenced by the PED-MS method as previously described.[46]

Equilibrium Binding Measurements. Equilibrium dissociation constants were determined by measuring the FA of 100 nm fluorescein-labeled CPs as a function of increasing concentrations of CA, WM CA-CTD, GagΔp6, or control proteins. The labeled peptides were incubated in amber tubes with varying amounts of the target protein for 2 h at RT in binding buffer (40 mM HEPES, pH 7.5, 150 mM NaCl, and 2 mM DTT). The binding of hLysRS to 100 nM Texas Red-labeled CA or WM CA-CTD was performed in a similar manner. All measurements were made on a Spectramax M5 plate reader (Molecular Devices). The wavelengths for monitoring excitation (Ex), emission (Em) and emission cut off (Co) for FITC and Texas Red were as follows: FITC, Ex = 494 nm, Em = 518 nm, and Co = 515 nm; Texas Red, Ex = 585 nm, Em = 620 nm, and Co = 610 nm. Slit widths of 5 nm were used all experiments. Data analysis was performed as previously described[24] by fitting the data to a 1:1 binding model with a correction for changes in fluorophore intensity due to protein binding (OriginPro 8 SRO). To confirm the binding stoichiometry of CP2 and CP4 to WM CA-CTD, increasing WM CA-CTD was added to a mixture of 10 μM fluorescein-labeled CP2 or CP4 and 590 μM unlabeled CP2 or CP4 in binding buffer. Changes in FA were monitored using a Spectramax M5 plate reader and wavelength settings for FITC as described above. Inhibition and competition assays are described in the Supporting Methods.

NMR Spectroscopy and Data Processing. Protein purification for NMR analysis is described in the Supporting Methods. All NMR spectra were collected at 25 °C on a Bruker 700 MHz spectrometer. Chemical shift assignments were achieved with the following NMR experiments: HNCA,[47−49] HNCACB,[50] CBCA(CO)NH,[51] HNCO,[48] TOCSY-HSQC,[52] and NOESY-HSQC.[53] For titration experiments, ^{1}H,^{15}N HSQC spectra of WM CA-CTD (100 μM or 250 μM) with 1:0, 1:1, 1:2, and 1:5 protein:spin-labeled peptide ratio were collected. The data were processed and analyzed using NMRPipe[54] and CARA.[55] Signal intensities were obtained from measuring the cross-peak intensity of each residue in the ^{1}H,^{15}N HSQC spectra using CARA[55] and were normalized using a internal reference signal. The intensity reduction ratios of each residue were calculated by dividing the signal intensity in the presence by that of the absence of spin-labeled peptides. The spin quenching experiment was performed in order to confirm that signal intensity changes were solely caused by spin-probe. In order to quench the free radicals of the spin-probe, 5-fold molar excess ascorbic acid was added into the mixture of WM CA-CTD and spin-labeled CPs (1:5 protein:peptide ratio). After the quenching, all signal intensities were restored to the values of the sample containing only WM CA-CTD. Therefore, signal intensity changes were caused by spin-label due to the interaction between CPs and WM CA-CTD.

ASSOCIATED CONTENT

⑤ Supporting Information

This material is available free of charge *via* the Internet at http://pubs.acs.org.

AUTHOR INFORMATION

Corresponding Author
*E-mail: musier@chemistry.ohio-state.edu; pei.3@osu.edu.

Author Contributions
○These authors contributed equally to this work.

Notes
The authors declare no competing financial interest.

ACKNOWLEDGMENTS

REFERENCES

(1) Rathbun, R. C., Lockhart, S. M., and Stephens, J. R. (2006) Current HIV treatment guidelines—an overview. *Curr. Pharm. Des. 12*, 1045−1063.

(2) Richman, D. D. (2001) HIV chemotherapy. *Nature 410*, 995−1001.

(3) Vierling, P., and Greiner, J. (2003) Prodrugs of HIV protease inhibitors. *Curr. Pharm. Des. 9*, 1755−1770.

(4) Tamalet, C., Yahi, N., Tourres, C., Colson, P., Quinson, A. M., Poizot-Martin, I., Dhiver, C., and Fantini, J. (2000) Multidrug resistance genotypes (insertions in the beta3-beta4 finger subdomain and MDR mutations) of HIV-1 reverse transcriptase from extensively treated patients: incidence and association with other resistance mutations. *Virology 270*, 310−316.

(5) Adamson, C. S., and Freed, E. O. (2010) Novel approaches to inhibiting HIV-1 replication. *Antiviral Res. 85*, 119−141.

(6) Mascarenhas, A. P., and Musier-Forsyth, K. (2009) The capsid protein of human immunodeficiency virus: interactions of HIV-1 capsid with host protein factors. *FEBS J. 276*, 6118−6127.

(7) Neira, J. L. (2009) The capsid protein of human immunodeficiency virus: designing inhibitors of capsid assembly. *FEBS J. 276*, 6110−6117.

(8) Kleiman, L., Jones, C. P., and Musier-Forsyth, K. (2010) Formation of the tRNALys packaging complex in HIV-1. *FEBS Lett. 584*, 359−365.

(9) Adamson, C. S., and Freed, E. O. (2007) Human immunodeficiency virus type 1 assembly, release, and maturation. *Adv. Pharmacol. 55*, 347−387.

(10) Ganser-Pornillos, B. K., Yeager, M., and Sundquist, W. I. (2008) The structural biology of HIV assembly. *Curr. Opin. Struct. Biol. 18*, 203−217.

(11) Gamble, T. R., Yoo, S., Vajdos, F. F., von Schwedler, U. K., Worthylake, D. K., Wang, H., McCutcheon, J. P., Sundquist, W. I., and Hill, C. P. (1997) Structure of the carboxyl-terminal dimerization domain of the HIV-1 capsid protein. *Science 278*, 849−853.

(12) von Schwedler, U. K., Stray, K. M., Garrus, J. E., and Sundquist, W. I. (2003) Functional surfaces of the human immunodeficiency virus type 1 capsid protein. *J. Virol. 77*, 5439−5450.

(13) Worthylake, D. K., Wang, H., Yoo, S., Sundquist, W. I., and Hill, C. P. (1999) Structures of the HIV-1 capsid protein dimerization domain at 2.6 A resolution. *Acta Crystallogr., Sect. D: Biol. Crystallogr. 55*, 85−92.

(14) Adamson, C. S., Salzwedel, K., and Freed, E. O. (2009) Virus maturation as a new HIV-1 therapeutic target. *Expert Opin. Ther. Targets 13*, 895−908.

(15) Hulme, A. E., Perez, O., and Hope, T. J. (2011) Complementary assays reveal a relationship between HIV-1 uncoating and reverse transcription. *Proc. Natl. Acad. Sci. U.S.A. 108*, 9975−9980.

(16) Ganser-Pornillos, B. K., von Schwedler, U. K., Stray, K. M., Aiken, C., and Sundquist, W. I. (2004) Assembly properties of the human immunodeficiency virus type 1 CA protein. *J. Virol. 78*, 2545−2552.

(17) Pornillos, O., Ganser-Pornillos, B. K., Kelly, B. N., Hua, Y., Whitby, F. G., Stout, C. D., Sundquist, W. I., Hill, C. P., and Yeager, M. (2009) X-ray structures of the hexameric building block of the HIV capsid. *Cell 137*, 1282−1292.

(18) Jiang, M., Mak, J., Ladha, A., Cohen, E., Klein, M., Rovinski, B., and Kleiman, L. (1993) Identification of tRNAs incorporated into wild-type and mutant human immunodeficiency virus type 1. *J. Virol. 67*, 3246−3253.

(19) Mak, J., and Kleiman, L. (1997) Primer tRNAs for reverse transcription. *J. Virol. 71*, 8087−8095.

(20) Javanbakht, H., Halwani, R., Cen, S., Saadatmand, J., Musier-Forsyth, K., Gottlinger, H., and Kleiman, L. (2003) The interaction between HIV-1 Gag and human lysyl-tRNA synthetase during viral assembly. *J. Biol. Chem. 278*, 27644−27651.

(21) Kobbi, L., Octobre, G., Dias, J., Comisso, M., and Mirande, M. (2011) Association of mitochondrial Lysyl-tRNA synthetase with HIV-1 GagPol involves catalytic domain of the synthetase and transframe and integrase domains of Pol. *J. Mol. Biol. 410*, 875−886.

(22) Halwani, R., Cen, S., Javanbakht, H., Saadatmand, J., Kim, S., Shiba, K., and Kleiman, L. (2004) Cellular distribution of Lysyl-tRNA synthetase and its interaction with Gag during human immunodeficiency virus type 1 assembly. *J. Virol. 78*, 7553−7564.

(23) Kovaleski, B. J., Kennedy, R., Khorchid, A., Kleiman, L., Matsuo, H., and Musier-Forsyth, K. (2007) Critical role of helix 4 of HIV-1 capsid C-terminal domain in interactions with human lysyl-tRNA synthetase. *J. Biol. Chem. 282*, 32274−32279.

(24) Kovaleski, B. J., Kennedy, R., Hong, M. K., Datta, S. A., Kleiman, L., Rein, A., and Musier-Forsyth, K. (2006) In vitro characterization of the interaction between HIV-1 Gag and human lysyl-tRNA synthetase. *J. Biol. Chem. 281*, 19449−19456.

(25) Guo, M., Shapiro, R., Morris, G. M., Yang, X. L., and Schimmel, P. (2010) Packaging HIV virion components through dynamic equilibria of a human tRNA synthetase. *J. Phys. Chem. B 114*, 16273−16279.

(26) Na Nakorn, P., Treesuwan, W., Choowongkomon, K., Hannongbua, S., and Boonyalai, N. (2011) In vitro and in silico binding study of the peptide derived from HIV-1 CA-CTD and LysRS as a potential HIV-1 blocking site. *J. Theor. Biol. 270*, 88−97.

(27) Tang, C., Loeliger, E., Kinde, I., Kyere, S., Mayo, K., Barklis, E., Sun, Y., Huang, M., and Summers, M. F. (2003) Antiviral inhibition of the HIV-1 capsid protein. *J. Mol. Biol. 327*, 1013−1020.

(28) Li, F., Goila-Gaur, R., Salzwedel, K., Kilgore, N. R., Reddick, M., Matallana, C., Castillo, A., Zoumplis, D., Martin, D. E., Orenstein, J. M., Allaway, G. P., Freed, E. O., and Wild, C. T. (2003) PA-457: a potent HIV inhibitor that disrupts core condensation by targeting a late step in Gag processing. *Proc. Natl. Acad. Sci. U.S.A. 100*, 13555−13560.

(29) Shi, J., Zhou, J., Shah, V. B., Aiken, C., and Whitby, K. (2011) Small-molecule inhibition of human immunodeficiency virus type 1 infection by virus capsid destabilization. *J. Virol. 85*, 542−549.

(30) Sticht, J., Humbert, M., Findlow, S., Bodem, J., Muller, B., Dietrich, U., Werner, J., and Krausslich, H. G. (2005) A peptide inhibitor of HIV-1 assembly in vitro. *Nat. Struct. Mol. Biol. 12*, 671−677.

(31) Zhang, H., Zhao, Q., Bhattacharya, S., Waheed, A. A., Tong, X., Hong, A., Heck, S., Curreli, F., Goger, M., Cowburn, D., Freed, E. O., and Debnath, A. K. (2008) A cell-penetrating helical peptide as a potential HIV-1 inhibitor. *J. Mol. Biol. 378*, 565−580.

768

dx.doi.org/10.1021/cb200450w | *ACS Chem. Biol.* 2012, 7, 761−769

(32) Bocanegra, R., Nevot, M., Domenech, R., Lopez, I., Abian, O., Rodriguez-Huete, A., Cavasotto, C. N., Velazquez-Campoy, A., Gomez, J., Martinez, M. A., Neira, J. L., and Mateu, M. G. (2011) Rationally designed interfacial peptides are efficient in vitro inhibitors of HIV-1 capsid assembly with antiviral activity. *PLoS One 6*, e23877.

(33) Hamada, Y., and Shioiri, T. (2005) Recent progress of the synthetic studies of biologically active marine cyclic peptides and depsipeptides. *Chem. Rev. 105*, 4441−4482.

(34) Laupacis, A., Keown, P. A., Ulan, R. A., McKenzie, N., and Stiller, C. R. (1982) Cyclosporin A: a powerful immunosuppressant. *Can.Med. Assoc. J. 126*, 1041−1046.

(35) Sandhu, P., Xu, X., Bondiskey, P. J., Balani, S. K., Morris, M. L., Tang, Y. S., Miller, A. R., and Pearson, P. G. (2004) Disposition of caspofungin, a novel antifungal agent, in mice, rats, rabbits, and monkeys. *Antimicrob. Agents Chemother. 48*, 1272−1280.

(36) Kirkpatrick, P., Raja, A., LaBonte, J., and Lebbos, J. (2003) Daptomycin. *Nat. Rev. Drug Discovery 2*, 943−944.

(37) Lalonde, M. S., Lobritz, M. A., Ratcliff, A., Chamanian, M., Athanassiou, Z., Tyagi, M., Wong, J., Robinson, J. A., Karn, J., Varani, G., and Arts, E. J. (2011) Inhibition of both HIV-1 reverse transcription and gene expression by a cyclic peptide that binds the Tat-transactivating response element (TAR) RNA. *PLoS Pathog 7*, e1002038.

(38) Chen, X., Tan, P. H., Zhang, Y., and Pei, D. (2009) On-bead screening of combinatorial libraries: reduction of nonspecific binding by decreasing surface ligand density. *J. Comb. Chem. 11*, 604−611.

(39) Wang, X., Peng, L., Liu, R., Xu, B., and Lam, K. S. (2005) Applications of topologically segregated bilayer beads in 'one-bead one-compound' combinatorial libraries. *J. Pept. Res. 65*, 130−138.

(40) Newman, J. L., Butcher, E. W., Patel, D. T., Mikhaylenko, Y., and Summers, M. F. (2004) Flexibility in the P2 domain of the HIV-1 Gag polyprotein. *Protein Sci. 13*, 2101−2107.

(41) Ternois, F., Sticht, J., Duquerroy, S., Krausslich, H. G., and Rey, F. A. (2005) The HIV-1 capsid protein C-terminal domain in complex with a virus assembly inhibitor. *Nat. Struct. Mol. Biol. 12*, 678−682.

(42) Liu, T., Joo, S. H., Voorhees, J. L., Brooks, C. L., and Pei, D. (2009) Synthesis and screening of a cyclic peptide library: discovery of small-molecule ligands against human prolactin receptor. *Bioorg. Med. Chem. 17*, 1026−1033.

(43) Wavreille, A. S., and Pei, D. (2007) A chemical approach to the identification of tensin-binding proteins. *ACS Chem. Biol. 2*, 109−118.

(44) Yoo, S., Myszka, D. G., Yeh, C., McMurray, M., Hill, C. P., and Sundquist, W. I. (1997) Molecular recognition in the HIV-1 capsid/cyclophilin A complex. *J. Mol. Biol. 269*, 780−795.

(45) Datta, S. A., and Rein, A. (2009) Preparation of recombinant HIV-1 gag protein and assembly of virus-like particles in vitro. *Methods Mol. Biol. 485*, 197−208.

(46) Joo, S. H., Xiao, Q., Ling, Y., Gopishetty, B., and Pei, D. (2006) High-throughput sequence determination of cyclic peptide library members by partial Edman degradation/mass spectrometry. *J. Am. Chem. Soc. 128*, 13000−13009.

(47) Matsuo, H., Kupce, E., Li, H., and Wagner, G. (1996) Increased sensitivity in HNCA and HN(CO)CA experiments by selective C beta decoupling. *J Magn. Reson. B 113*, 91−96.

(48) Kay, L., Ikura, M., Tschudin, R., and Bax, A. (1990) Three-dimensional triple-resonance NMR spectroscopy of isotopically enriched proteins. *J. Magn. Reson. 89*, 18.

(49) Ikura, M., Kay, L. E., and Bax, A. (1990) A novel approach for sequential assignment of 1H, 13C, and 15N spectra of proteins: heteronuclear triple-resonance three-dimensional NMR spectroscopy. Application to calmodulin. *Biochemistry 29*, 4659−4667.

(50) Wittekind, M., and Mueller, J. D. (1993) HNCACB, a highsensitivity 3D NMR experiment to correlate amideproton and nitrogen resonances with the alpha- and beta-carbon resonances in proteins. *J. Magn. Reson. 101*, 4.

(51) Grzesiek, S., and Bax, A. (1992) Correlating backbone amide and side chain resonances in larger proteins by multiple relayed triple resonance NMR. *J. Am. Chem. Soc. 114*, 3.

(52) Wijmenga, S. S., van Mierlo, C. P., and Steensma, E. (1996) Doubly sensitivity-enhanced 3D TOCSY-HSQC. *J. Biomol. NMR 8*, 319−330.

(53) Zhang, O., Kay, L. E., Olivier, J. P., and Forman-Kay, J. D. (1994) Backbone 1H and 15N resonance assignments of the N-terminal SH3 domain of drk in folded and unfolded states using enhanced-sensitivity pulsed field gradient NMR techniques. *J. Biomol. NMR 4*, 845−858.

(54) Delaglio, F., Grzesiek, S., Vuister, G. W., Zhu, G., Pfeifer, J., and Bax, A. (1995) NMRPipe: a multidimensional spectral processing system based on UNIX pipes. *J. Biomol. NMR 6*, 277−293.

(55) Keller, R. L. J. (2004) *The Computer Aided Resonance Assignment Tutorial*, p 81, Cantina Verlag, Switzerland.

(56) DeLano, W. L. (2002) *The PyMOL Molecular Graphics System*, DeLano Scientific, San Carlos, CA.